REGULARIZATION DESIGN FOR ISOTROPIC SPATIAL RESOLUTION IN MOTION-COMPENSATED IMAGE RECONSTRUCTION

Se Young Chun[1] *and Jeffrey A. Fessler*[2]

[1] Radiology, Massachusetts General Hospital and Harvard Medical School, USA
[2] Electrical Engineeing and Computer Science, University of Michigan, Ann Arbor, USA

ABSTRACT

Patient motion degrades image quality in medical imaging. Gating can reduce motion artifacts by using part of the acquired data, but can increase noise. Motion-compensated image reconstruction (MCIR) utilizes all collected data with motion information to reduce motion artifacts *and* noise.

Interactions between Poisson log-likelihood and quadratic regularizers lead to nonuniform and anisotropic spatial resolution in the static case. These undesirable problems can become worse in MCIR due to local motion. We previously compensated for local volume changes in MCIR to provide approximately uniform spatial resolution, but achieved isotropic resolution only for the static case.

This paper proposes a quadratic spatial regularizer design that achieves nearly uniform and isotropic spatial resolution in MCIR. We consider "analytical approach" to regularization design that was developed for static image reconstruction and extend it to MCIR methods based on a general parametric motion model. Our proposed regularizer can compensate not only for the effects of interactions between the Poisson log-likelihood and the spatial regularizer but also for the effects of nonrigid motion. A 2D PET simulation demonstrates the theoretical results.

1. INTRODUCTION

Motion is an important problem in many medical imaging modalities such as PET, SPECT, and CT. Due to their innate acquisition time (and dose) limitations, there are tradeoffs between image noise (SNR) and motion artifacts. Gating methods can reduce motion artifacts, but they also reduce SNR or decrease radiation dose efficiency by discarding potentially useful data.

Motion-compensated image reconstruction (MCIR) methods attempt to use all collected data and motion information to improve image quality. Many such methods use nonrigid motion models that can be estimated separately [1–3], or simultaneously [4, 5]. Such methods can improve SNR and reduce motion artifacts.

This work is supported in part by 1P01 CA87634.

Interactions between the log-likelihood for Poisson measurements and conventional quadratic regularizers leads to nonuniform and anisotropic spatial resolution [6]. There are methods for designing quadratic regularizers that can achieve uniform and isotropic spatial resolution in the static case [7, 8]. Resolution non-uniformity and anisotropy problems can worsen in MCIR due to local motion. There are a few methods for achieving approximately uniform spatial resolution in MCIR methods [9, 10], but resolution anisotropy has not be addressed previously.

This paper proposes a method for 2D quadratic spatial regularization design that provides approximately uniform and isotropic spatial resolution in MCIR. We consider the "analytical approach" to isotropic spatial regularization design that was developed for static imaging [8] and extend it to MCIR methods based on a general parametric motion model. Our proposed regularizer can compensate not only for the effects of interactions between the Poisson log-likelihood and the spatial regularizer but also for the effects of nonrigid motions. A 2D PET simulation with affine motion illustrates the theory.

2. METHOD

2.1. Measurement model

Let $\boldsymbol{f}_m,\ m = 1, \ldots, M$ denote the object in the mth frame in a gated study. We assume the following measurement model:

$$\boldsymbol{y}_m = \boldsymbol{G}\boldsymbol{f}_m + \boldsymbol{\epsilon}_m, \tag{1}$$

where $\boldsymbol{y}_m$ denotes the measurements for the mth frame, $\boldsymbol{G}$ denotes the system model and $\boldsymbol{\epsilon}_m$ denotes noise (possibly Poisson). We assume that the object $\boldsymbol{f}_m$ and measurement $\boldsymbol{y}_m$ are motion-free, *i.e.*, the object does not move during the mth scan (gate or frame).

2.2. Motion and warp model

Without loss of generality, we assume that $\boldsymbol{f}_1$ is our reference image frame among $\{\boldsymbol{f}_1, \cdots, \boldsymbol{f}_M\}$. Then, the rest of the image frames are represented as a warped version of $\boldsymbol{f}_1$:

$$\boldsymbol{f}_m = \boldsymbol{T}_m \boldsymbol{f}_1, \qquad m = 1, \ldots, M, \tag{2}$$

where $\boldsymbol{T}_m$ is an image interpolation operator with the corresponding transformation that maps $f_1(\underline{x})$ to $f_m(\underline{x})$, *i.e.*, $f_m(\underline{x}) = f_1(T_m(\underline{x}))$.

For many medical imaging modalities, a warp (2) usually preserves mass or activity. In this paper, we adopt this mass-preserving property and the new mass-preserving warp is:

$$\boldsymbol{f}_m = \mathring{\boldsymbol{T}}_m \boldsymbol{f}_1 \triangleq \boldsymbol{D}(|\nabla T_m(\underline{x}_j)|)\boldsymbol{T}_m \boldsymbol{f}_1 \tag{3}$$

where $\boldsymbol{D}(\cdot)$ is a diagonal matrix. One can show that the transpose of $\mathring{\boldsymbol{T}}_m$ is $\mathring{\boldsymbol{T}}'_m \approx \boldsymbol{T}_m^{-1}$.

2.3. Motion-compensated image reconstruction model

Substituting (3) into (1) yields a measurement model that depends only on one image $\boldsymbol{f}_1$ instead of all images $\boldsymbol{f}_m$:

$$\boldsymbol{y}_m = \boldsymbol{G}\mathring{\boldsymbol{T}}_m \boldsymbol{f}_1 + \boldsymbol{\epsilon}_m, \quad m = 1, \dots, M.$$

Stacking up these models lead to the overall model

$$\boldsymbol{y}_{\mathrm{c}} = \boldsymbol{G}_{\mathrm{d}} \mathring{\boldsymbol{T}}_{\mathrm{c}} \boldsymbol{f}_1 + \boldsymbol{\epsilon}_{\mathrm{c}}, \tag{4}$$

where $\boldsymbol{y}_{\mathrm{c}} = [\boldsymbol{y}'_1, \cdots, \boldsymbol{y}'_M]'$, $\boldsymbol{G}_{\mathrm{d}} = \mathrm{diag}\{\boldsymbol{G}, \cdots, \boldsymbol{G}\}$, $\mathring{\boldsymbol{T}}_{\mathrm{c}} = [\mathring{\boldsymbol{T}}'_1, \cdots, \mathring{\boldsymbol{T}}'_M]'$, and $\boldsymbol{\epsilon}_{\mathrm{c}} = [\boldsymbol{\epsilon}'_1, \cdots, \boldsymbol{\epsilon}'_M]'$. One can determine $\mathring{\boldsymbol{T}}_{\mathrm{c}}$ from the measurements $\boldsymbol{y}_{\mathrm{c}}$ or from other measurements, *e.g.*, from CT in PET-CT systems or from MR in PET-MR. Here we treat $\mathring{\boldsymbol{T}}_{\mathrm{c}}$ as predetermined (known).

One can use (4) with any statistical image reconstruction approach such as penalized likelihood (PL). Here, we use a penalized weighted least square (PWLS) function:

$$\begin{aligned} \hat{\boldsymbol{f}}_{\mathrm{MCIR}} &\triangleq \underset{\boldsymbol{f}_1}{\mathrm{argmin}} \|\boldsymbol{y}_{\mathrm{c}} - \boldsymbol{G}_{\mathrm{d}} \mathring{\boldsymbol{T}}_{\mathrm{c}} \boldsymbol{f}_1\|^2_{\boldsymbol{W}_{\mathrm{d}}} + \eta \|\boldsymbol{C}\boldsymbol{f}_1\|^2 \qquad (5) \\ &= [\mathring{\boldsymbol{T}}_{\mathrm{c}}{}' \boldsymbol{G}'_{\mathrm{d}} \boldsymbol{W}_{\mathrm{d}} \boldsymbol{G}_{\mathrm{d}} \mathring{\boldsymbol{T}}_{\mathrm{c}} + \eta \boldsymbol{R}]^{-1} \mathring{\boldsymbol{T}}_{\mathrm{c}}{}' \boldsymbol{G}'_{\mathrm{d}} \boldsymbol{W}_{\mathrm{d}} \boldsymbol{G}_{\mathrm{d}} \mathring{\boldsymbol{T}}_{\mathrm{c}} \boldsymbol{f}_1, \end{aligned}$$

where $\boldsymbol{W}_{\mathrm{d}} = \mathrm{diag}\{\boldsymbol{W}_1, \cdots, \boldsymbol{W}_M\}$, $\boldsymbol{W}_m$ is a weight matrix that approximates the inverse of the covariance of $\boldsymbol{y}_m$, η is a regularization parameter. Independence of the measurements $\boldsymbol{y}_{\mathrm{c}}$ leads to $\mathring{\boldsymbol{T}}_{\mathrm{c}}{}' \boldsymbol{G}'_{\mathrm{d}} \boldsymbol{W}_{\mathrm{d}} \boldsymbol{G}_{\mathrm{d}} \mathring{\boldsymbol{T}}_{\mathrm{c}} = \sum_{m=1}^M \mathring{\boldsymbol{T}}'_m \boldsymbol{G} \boldsymbol{W}_m \boldsymbol{G} \mathring{\boldsymbol{T}}_m$. In here, we focus on quadratic regularization methods using first-order differences as follows:

$$\boldsymbol{R}\boldsymbol{f}_1 = \boldsymbol{C}'\boldsymbol{C}\boldsymbol{f}_1 \triangleq \sum_{m,n} \sum_{l=1}^L r_l^j ((c_l ** f_1)[n,m])^2, \tag{6}$$

where $**$ denotes 2D convolution, $f_1[n,m]$ denotes the 2D array corresponding to the lexicographically ordered vector $\boldsymbol{f}_1$, j is the lexicographic index to the pixel at $[n,m]$ and

$$c_l[n,m] = \frac{1}{\sqrt{n_l^2 + m_l^2}} (\delta_2[n,m] - \delta_2[n - n_l, m - m_l]), \tag{7}$$

where $\{(n_l, m_l)\}$ denote the offsets of the jth pixel's neighbors and $\delta_2[n,m]$ denote the 2D Kronecker impulse. In here, we used $\{(n_l, m_l)\} = \{(1,0), (0,1), (1,1), (1,-1)\}$.

2.4. Regularization design

For a single-frame estimator $\hat{\boldsymbol{f}}_m(\boldsymbol{y}_m)$ based on (1), one can define a local impulse response (LIR) for the jth pixel as [6]:

$$\boldsymbol{l}_m^j = \lim_{\delta \to 0} \frac{\hat{\boldsymbol{f}}_m(\boldsymbol{y} + \delta \boldsymbol{G} e_j) - \hat{\boldsymbol{f}}_m(\boldsymbol{y})}{\delta}.$$

Similarly, one can derive the LIR of MCIR estimator (5) as:

$$\boldsymbol{l}^j_{\mathrm{MCIR}} = [\mathring{\boldsymbol{T}}_{\mathrm{c}}{}' \boldsymbol{G}'_{\mathrm{d}} \boldsymbol{W}_{\mathrm{d}} \boldsymbol{G}_{\mathrm{d}} \mathring{\boldsymbol{T}}_{\mathrm{c}} + \boldsymbol{R}]^{-1} \mathring{\boldsymbol{T}}_{\mathrm{c}}{}' \boldsymbol{G}'_{\mathrm{d}} \boldsymbol{W}_{\mathrm{d}} \boldsymbol{G}_{\mathrm{d}} \mathring{\boldsymbol{T}}_{\mathrm{c}} e_j.$$

We would like to design the regularizer $\boldsymbol{R}$ (*i.e.*, to select r_l^j in (6)) so that the LIR closely matches some target point spread function (PSF). A reasonable target for the jth pixel [8] is

$$\boldsymbol{l}_0^j = [\boldsymbol{G}'\boldsymbol{G} + \boldsymbol{R}_0]^{-1} \boldsymbol{G}'\boldsymbol{G} e_j \tag{8}$$

which is the (often shift-invariant) LIR of a penalized unweighted least square (PULS) estimator, and $\boldsymbol{R}_0$ denotes a conventional shift-invariant regularizer. If we assume slowly varying weights in $\boldsymbol{W}_m$ [8] and locally affine motion for non-rigid motion $\boldsymbol{T}_m$ at the jth pixel, then $\mathring{\boldsymbol{T}}_{\mathrm{c}}{}' \boldsymbol{G}'_{\mathrm{d}} \boldsymbol{W}_{\mathrm{d}} \boldsymbol{G}_{\mathrm{d}} \mathring{\boldsymbol{T}}_{\mathrm{c}}$ becomes approximately a locally circulant matrix. By an argument similar to [8], one can show that "$\boldsymbol{l}^j_{\mathrm{MCIR}} = \boldsymbol{l}^j_0$" reduces to

$$\boldsymbol{R}_0 \sum_{m=1}^M \mathring{\boldsymbol{T}}'_m \boldsymbol{G}' \boldsymbol{W}_m \boldsymbol{G} \mathring{\boldsymbol{T}}_m e_j \approx \boldsymbol{R}\boldsymbol{G}'\boldsymbol{G} e_j. \tag{9}$$

Therefore, our regularization design becomes an optimization problem as follows for all j:

$$\min_{\{r_l^j\}_{l=1}^L} \left\| \boldsymbol{R}_0 \sum_{m=1}^M \mathring{\boldsymbol{T}}'_m \boldsymbol{G}' \boldsymbol{W}_m \boldsymbol{G} \mathring{\boldsymbol{T}}_m e_j - \boldsymbol{R}\boldsymbol{G}'\boldsymbol{G} e_j \right\|_2. \tag{10}$$

2.5. Analytical formulation

To simplify the matrix formulation (10), we extend the analytical approach of [8] to the MCIR case. For $\mathring{\boldsymbol{T}}_m = \boldsymbol{I}$, the analytical form of (10) is well defined in [8]. For a polar coordinates (ρ, φ) in frequency space, $\boldsymbol{G}'\boldsymbol{G} \equiv |B(\rho)|^2 / \rho$ where $B(\cdot)$ denotes the frequency response of a typical radial blur function $b(r)$. For a standard quadratic penalty function $\boldsymbol{R}_0$ (*i.e.* $\int \|\nabla f_1\|^2$), one can show that $\boldsymbol{R}_0 \equiv (2\pi\rho)^2$, and the quadratic funtion $\boldsymbol{R}$, *i.e.* (6), becomes $\boldsymbol{R} \equiv \sum_{l=1}^L r_l^j (2\pi\rho)^2 \cos^2(\varphi - \varphi_l)$, where $\varphi_l = \tan^{-1}(m_l / n_l)$. One can also show that

$$\boldsymbol{G}'\boldsymbol{W}_m\boldsymbol{G} \equiv \omega^j(\varphi) \left| B^j_\varphi(\rho) \right|^2 / \rho, \tag{11}$$

where $B^j_\varphi(\cdot)$ denotes the frequency response of the detector response $b^j_\varphi(r)$ at angle φ local to where the jth pixel projects onto the detector at that angle and $\omega^j(\varphi)$ denotes the effective certainty $\omega^j(\varphi) = \int_{-\infty}^\infty |b^j_\varphi(r)|^2 \omega_\varphi(r)\, \mathrm{d}r / \int_{-\infty}^\infty |b^j_\varphi(r)|^2\, \mathrm{d}r$. For static case $\mathring{\boldsymbol{T}}_m = \boldsymbol{I}$, [8] showed that (10) becomes

$$\min_{\{r_l^j\}_{l=1}^L} \int_0^\pi \left(\bar{\omega}^j(\varphi) - \sum_{l=1}^L r_l^j \cos^2(\varphi - \varphi_l) \right)^2 \mathrm{d}\varphi, \tag{12}$$

where the angular-dependent weighting for the jth pixel is

$$\bar{\omega}^j(\varphi) = \int_{-\infty}^{\infty} |b_\varphi^j(r)|^2 \omega_\varphi(r)\,\mathrm{d}r \Big/ \int_{-\infty}^{\infty} |b(r)|^2\,\mathrm{d}r \quad (13)$$

To analyze the effect of motion on (11) and (13), we used a continuous analogue of $\mathring{\boldsymbol{T}}'_m \boldsymbol{G}' \boldsymbol{W}_m \boldsymbol{G} \mathring{\boldsymbol{T}}_m \boldsymbol{f}_1$ near the jth pixel with a locally affine motion approximation and ignoring blurring as follows:

$$f(\underline{x}') * * \int_0^\pi \omega(\varphi)\delta(T^{-1}(\underline{x}') \cdot (\cos\varphi, \sin\varphi))\,\mathrm{d}\varphi \Big|_{\underline{x}'=\underline{x}}, \quad (14)$$

where $\omega(\varphi) \triangleq \omega_\varphi(T^{-1}(\underline{x}) \cdot (\cos\varphi, \sin\varphi))$. Similar to the scaling property of the Dirac impulse, one can approximate $\delta(T^{-1}(\underline{x}) \cdot \underline{h})/|\nabla T(\underline{x})| \approx \delta(\underline{x} \cdot \underline{h})$, and

$$\mathring{\boldsymbol{T}}'_m \boldsymbol{G}' \boldsymbol{W}_m \boldsymbol{G} \mathring{\boldsymbol{T}}_m \equiv |\nabla T(\underline{x}_j)| \omega^{j'}(\varphi) \left| B_\varphi^{j'}(\rho) \right|^2 \Big/ \rho,$$

where $B_\varphi^{j'}(\cdot)$ denotes the frequency response of the $b_\varphi^{j'}(r)$ at angle φ local to where the pixel at $T^{-1}(\underline{x}_j)$ projects onto the detector at that angle and $\omega^{j'}(\varphi)$ denotes the effective certainty corresponding to $b_\varphi^{j'}(r)$. Thus, (13) becomes

$$\bar{\omega}^j_{\mathrm{MCIR}}(\varphi) = |\nabla T(\underline{x}_j)| \bar{\omega}^{j'}(\varphi) \quad (15)$$

which is

$$\sum_m |\nabla T_m(\underline{x}_j)| \sum_k [t_m]_{kj} \sum_{i \in \mathcal{I}_\varphi} a_{ik}^2 [\omega_m]_i \Big/ \sum_{i \in \mathcal{I}_\varphi} a_{ij}^2 \quad (16)$$

where $\boldsymbol{G} = \{a_{ij}\}$, $\mathring{\boldsymbol{T}}_m = \{[t_m]_{ij}\}$, $\boldsymbol{W}_m = \mathrm{diag}\,\{[\omega_m]_i\}$, and $\mathcal{I}_\varphi$ denotes the set of rays that correspond to the projection at angle φ. The key is that (16) accounts for local motion effects.

We can replace $\bar{\omega}^j(\varphi)$ in (12) with (16) and solving (12) analytically is described in [8]. We use the same analytical approach with (15) instead of (13). We omit the description here due to space limits.

3. SIMULATION RESULTS

We generated a simple phantom with two high intensity rings and warped it with 3 different count-preserving affine transformations. We chose affine motion for illustration, but the theory applies to any nonrigid motion because a Taylor expansion can approximate nonrigid motion locally as affine motion. The original image has 160×160 pixels with 3.4 mm pixel size in Fig. 1. We forward projected these original images using a PET scanner geometry with 164 detector samples with 3.4 mm spacing 120 angular views, 3.4 mm strip width to model detector response and 5% random coincidences. We used a uniform attenuation map over the object.

To study spatial resolution, we reconstructed images from these 4 noiseless sinograms using four methods: PULS (Target), PWLS with a constant quadratic regularizer (Standard), PWLS with a certainty based regularizer considering Jacobian determinant [10] (Certainty9), and the proposed method (Proposed) based on (16). We used a preconditioned conjugate gradient method for all optimizations.

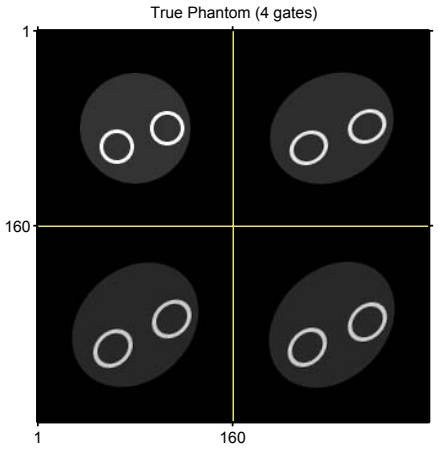

Fig. 1. Four true phantom images with affine motion.

Fig. 2 shows that the Standard approach yields highly nonuniform resolution. Certainty9 reduced this nonuniformity, but the rings still have nonuniform intensity due to the anisotropic PSF. The Proposed method yields nearly uniform intensities around the rings, as desired, and matches the Target closely. Fig. 3 shows profiles around the rings; our Proposed approach closely matches the target resolution.

Fig. 4 shows that motion can further skew the PSF (Standard) compared to the PSF without motion (Standard1, one gate). Certainty9 was designed to achieve uniform spatial resolution but it still has an anisotropic shape. The Proposed PSF matches the Target PSF approximately.

4. DISCUSSION

This paper proposed a 2D quadratic regularization design for MCIR methods. The proposed regularizer efficiently utilizes the analytical approach to spatial regularizer design with a simple modification of the static version in [8]. The results show that our proposed regularizer can achieve the nearly uniform and isotropic PSFs even in the presence of large anisotropic motion.

Natural future work includes evaluation with more general nonrigid motion and extending the theory to 3D. This approach can also be used to design a regularizer for fan-beam geometry by modeling the warp between fan-beam and parallel-beam coordinates. By composing the geometry warp and nonrigid patient motion, one may be able to design regularizers that compensate for both motion and non-parallel geometries simultaneously. We also expect to be able to predict noise properties of MCIR methods using this type of analysis.

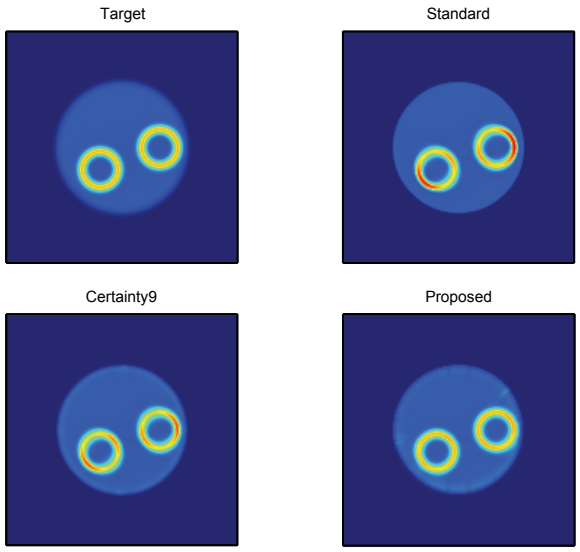

Fig. 2. In Standard, uneven intensity around rings can be observed even though True Phantom and Target have uniform intensities. Proposed approach achieves approximately uniform intensity around the rings.

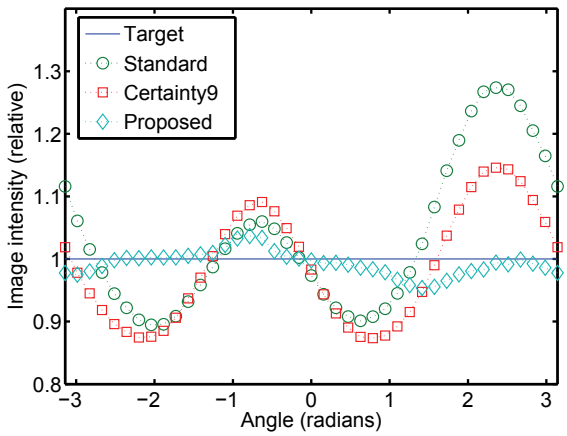

Fig. 3. Profiles around the left ring. The Proposed approach closely matches the target image.

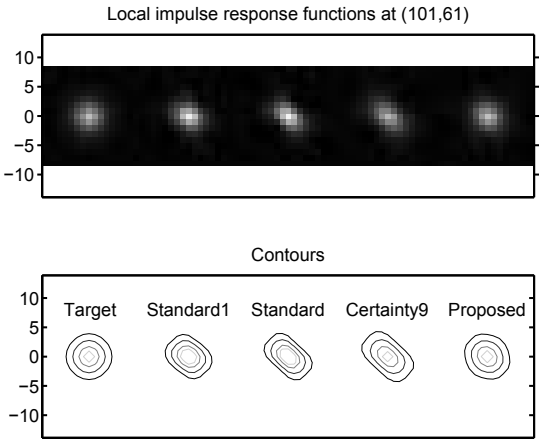

Fig. 4. Local impulse response functions at pixel (101,61). Standard1 with one gate and Standard with 4 gates show that affine motions affect the shape of PSFs. Proposed corrects the anisotropy caused both by motion and by data-dependent weights.

5. REFERENCES

[1] F. Qiao, T. Pan, J. W. Clark, and O. R. Mawlawi, "A motion-incorporated reconstruction method for gated PET studies," *Phys. Med. Biol.*, vol. 51, no. 15, pp. 3769–84, Aug. 2006.

[2] T. Li, B. Thorndyke, E. Schreibmann, Y. Yang, and L. Xing, "Model-based image reconstruction for four-dimensional PET," *Med. Phys.*, vol. 33, no. 5, pp. 1288–98, May 2006.

[3] F. Lamare, M. J. Ledesma Carbayo, T. Cresson, G. Kontaxakis, A. Santos, C. Cheze LeRest, A. J. Reader, and D. Visvikis, "List-mode-based reconstruction for respiratory motion correction in PET using non-rigid body transformations," *Phys. Med. Biol.*, vol. 52, no. 17, pp. 5187–204, Sept. 2007.

[4] M. W. Jacobson and J. A. Fessler, "Joint estimation of image and deformation parameters in motion-corrected PET," in *Proc. IEEE Nuc. Sci. Symp. Med. Im. Conf.*, 2003, vol. 5, pp. 3290–4.

[5] K. Taguchi, M. Zhang, E. C. Frey, J. Xu, W. Paul Segars, and B. M. W. Tsui, "Image-domain material decomposition using photon-counting CT," in *Proc. SPIE 6510, Medical Imaging 2007: Phys. Med. Im.*, 2007, p. 651008.

[6] J. A. Fessler and W. L. Rogers, "Spatial resolution properties of penalized-likelihood image reconstruction methods: Space-invariant tomographs," *IEEE Trans. Im. Proc.*, vol. 5, no. 9, pp. 1346–58, Sept. 1996.

[7] J. Nuyts and J. A. Fessler, "A penalized-likelihood image reconstruction method for emission tomography, compared to post-smoothed maximum-likelihood with matched spatial resolution," *IEEE Trans. Med. Imag.*, vol. 22, no. 9, pp. 1042–52, Sept. 2003.

[8] H. R. Shi and J. A. Fessler, "Quadratic regularization design for 2D CT," *IEEE Trans. Med. Imag.*, vol. 28, no. 5, pp. 645–56, May 2009.

[9] E. Asma, R. Manjeshwar, and K. Thielemans, "Theoretical comparison of motion correction techniques for PET image reconstruction," in *Proc. IEEE Nuc. Sci. Symp. Med. Im. Conf.*, 2006, vol. 3, pp. 1762–7.

[10] S. Y. Chun and J. A. Fessler, "Spatial resolution and noise properties of regularized motion-compensated image reconstruction," in *Proc. IEEE Intl. Symp. Biomed. Imag.*, 2009, pp. 863–6.